Arabian Journal of Chemistry (2022) **15**, 104316

King Saud University

Arabian Journal of Chemistry

www.ksu.edu.sa
www.sciencedirect.com

ORIGINAL ARTICLE

Facile synthesis and characterization of copper oxalate/cobalt oxalate/manganese oxalate and copper oxide/cobalt manganese oxide/manganese oxide as new nanocomposites for efficient photocatalytic degradation of malachite green dye

Reem K. Shah [a], **Salwa AlReshaidan** [b,*]

[a] *Department of Chemistry, Faculty of Applied Sciences, Umm Al-Qura University, Makkah 21955, Saudi Arabia*
[b] *Department of Chemistry, Faculty of Science, King Saud University, Riyadh 11451, Saudi Arabia*

Received 3 August 2022; accepted 27 September 2022
Available online 3 October 2022

KEYWORDS

Nanoparticles;
Photocatalytic degradation;
Analytical parameters;
Malachite green dye

Abstract Scientists seek to synthesize new catalysts with simple methods to treat water pollution from organic dyes using photocatalytic degradation technology. In this technology, when light falls on the catalyst, the produced hydroxyl free radicals convert the dye into non-toxic gases such as CO_2 and H_2O. So, in this work, copper oxalate/cobalt oxalate/manganese oxalate (Abbreviated as P_1) and copper oxide/cobalt manganese oxide/manganese oxide (Abbreviated as P_2) new nanocomposites were fabricated via precipitation of $Cu^{2+}/Co^{2+}/Mn^{2+}$ solution using oxalic acid and ignition of precipitate at 550 °C for 4 hrs, respectively. Some tools, involving X-ray diffraction (XRD), UV–vis spectrophotometer, energy dispersive X-ray spectroscopy (EDX), nitrogen gas sorption analyzer, transmission electron microscope (TEM), and field emission scanning electron microscope (FE-SEM), were used for characterizing the fabricated nanocomposites. The EDX spectra confirmed that the P_1 composite consist of C (26.28 %), oxygen (46.66 %), manganese (7.27 %), cobalt (7.59 %), and copper (12.20 %). Also, the P_2 composite consist of oxygen (8.23 %), manganese (31.34 %), cobalt (27.19 %), and copper (33.24 %). A transmission electron microscope shows that the P_1 and P_2 composites consist of polyhedral and spherical shapes with an average diameter of 28.13 and 14.37 nm, respectively. The BET surface area, average pore size, and total pore volume of the P_1 composite are 29.0725 m^2/g, 2.0749 nm, and 0.0302 cc/g, respectively.

* Corresponding author.
E-mail address: chem241@ksu.edu.sa (S. AlReshaidan).
Peer review under responsibility of King Saud University.

Production and hosting by Elsevier

https://doi.org/10.1016/j.arabjc.2022.104316

Besides, the BET surface area, average pore size, and total pore volume of the P_2 composite are 58.1088 m^2/g, 1.6087 nm, 0.0467 cc/g, respectively. 60 mg of the synthesized nanocomposites completely decompose 60 mL of 15 mg/L of malachite green dye solution within 20 min in the presence of hydrogen peroxide and UV light. The synthesized catalysts outperformed many other catalysts published in previous studies.

1. Introduction

Water contamination by harmful industrial wastes is the most serious environmental issue. Numerous approaches and substances are being researched to purify the water (Adel et al., 2022; Bi et al., 2022; Rayaroth et al., 2022). Thousands of synthetic dyes are the primary cause of water pollution. Since the majority of these dyes are non-biodegradable, they stay in the water for an extended period of time. In addition to their toxicity, even low quantities of these substances harm aquatic life by blocking sunlight. Malachite green is among the industrial organic dyes that are harmful to mammalian cells. Malachite green is a dye used in the paper, cotton, jute, wool, silk, leather, and acrylic industries, as well as an antibacterial and fungicide (Raval et al., 2017). Since the pollutants are transformed from one phase to another in the adsorption method, a secondary pollutant issue occurs despite the fact that adsorption methods are the most extensively utilized for dye removal as they are efficient and economical (Abdelrahman, 2018; Abdelrahman et al., 2019a). Consequently, intensive research is being conducted on the removal of contaminants via photodegradation (Abdelrahman et al., 2019b; Alharbi and Abdelrahman, 2020; Hegazey et al., 2020). In recent years, advanced oxidation technologies have been utilized efficiently for the degradation of hazardous chemicals in wastewater (Abdelrahman and Hegazey, 2019). Using semiconductor catalyst, heterogeneous photocatalysis completely converts organic contaminants to CO_2 and H_2O with the help of the generated free radicals (Abdelrahman and Hegazey, 2019). There are many catalysts for degrading malachite green dyes such as Fe(III)-cross-linked alginate-carboxymethyl cellulose composite (Karadeniz et al., 2022), cobalt oxide/citric acid nanocomposite (Verma et al., 2021), sn-doped TiO_2 (Sayilkan et al., 2007), Fe_3O_4/ SiO_2/TiO_2 composite (Farhadian and Kazemzad, 2016), and chitosan supported Ce–ZnO (Saad et al., 2020). However, most of these catalysts require a high cost to prepare them, as well as their ability to degrade a small concentration of malachite green dye in a large time. Therefore, scientists strive to prepare effective catalysts in simple ways using low-cost chemicals. Copper, cobalt, and manganese salts are cheap, available, and easy to purchase. Also, oxalic acid is among the cheapest organic precipitants for the preparation of low crystalline nanomaterials. Precipitation and/or ignition method is an effective method for producing many nanomaterials such as iron oxide (AL-Harbi and Darwish, 2022), ferromagnetic nanoparticles (Kumar and Gangawane, 2022), zinc oxide (Mahmood et al., 2022), Mn_3O_4 (Altiner et al., 2022), cerium oxide (Aseena et al., 2021), borohydride (Wang and Aguey-Zinsou, 2021), $CuCo_2O_4$ (Sun et al., 2021), and cadmium oxide (Sujatha et al., 2021). So, in this work, copper oxalate/cobalt oxalate/manganese oxalate and copper oxide/cobalt manganese oxide/manganese oxide new nanocomposites were synthesized by precipitation of Cu^{2+}/Co^{2+}/Mn^{2+} solution using oxalic acid and ignition of precipitate at 550 °C for 4 hrs, respectively. Some tools, involving X-ray diffraction (XRD), UV–vis spectrophotometer, energy

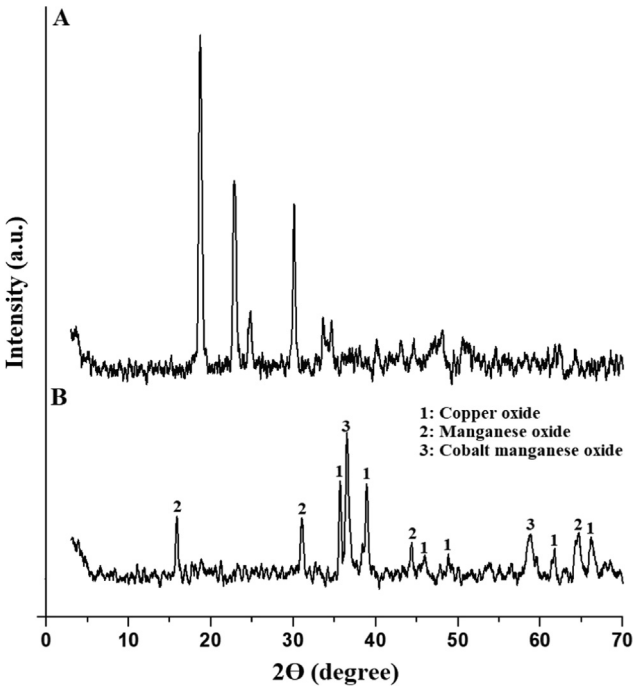

Fig. 1 XRD patterns of the P_1 (A) and P_2 (B) composites.

Table 1 Parameters affecting the photocatalytic degradation of malachite green dye using the P_1 and P_2 composites.

Parameter	Experimental conditions				
	Concentration of dye (mg/L)	Volume of dye (mL)	Amount of catalyst (mg)	Irradiation time (min)	pH
pH (2.5–8.5)	15	60	60	180	——
Time (4–40 min)	15	60	60	——	8.5
Amount of catalyst (0.02–0.1 g)	15	60	——	32 min and 20 min in the absence and presence of H_2O_2, respectively.	8.5
Concentration of dye (5–25 mg/L)	—	60	60	32 min and 20 min in the absence and presence of H_2O_2, respectively.	8.5
Regeneration and reusability	15	60	60	32 min and 20 min in the absence and presence of H_2O_2, respectively.	8.5

dispersive X-ray spectroscopy (EDX), nitrogen gas sorption analyzer, transmission electron microscope (TEM), and field emission scanning electron microscope (FE-SEM), were used for characterizing the fabricated nanocomposites. The produced nanocomposites were employed as new photocatalysts for the degradation of malachite green dye. Furthermore, analytical parameters impacting the degradation efficiency of malachite green dye, such as pH, irradiation time, dye concentration, and catalyst quantity, have been investigated.

2. Experimental

2.1. Utilized chemicals

Copper(II) acetate monohydrate ($Cu(CH_3COO)_2{\cdot}H_2O$), cobalt (II) acetate tetrahydrate ($Co(CH_3COO)_2{\cdot}4H_2O$), hydrochloric acid (HCl), oxalic acid ($C_2H_2O_4$), sodium hydroxide (NaOH), manganese(II)acetate tetrahydrate ($Mn(CH_3COO)_2{\cdot}4H_2O$), hydrogen peroxide ($H_2O_2$), and malachite green dye ($C_{23}H_{25}ClN_2$) were acquired from Sigma Aldrich Company (Purity = 99.99 %) and utilized without further purification.

2.2. Synthesis of composites

5.00 g of copper(II) acetate monohydrate, 5.00 g of manganese (II) acetate tetrahydrate, and 5.00 g of cobalt(II) acetate tetrahydrate were dissolved in 250 mL of distilled water for getting the Cu/Co/Mn solution. Additionally, 8.50 g of oxalic acid was dissolved in 120 mL of distilled water. After that, the oxalic acid solution was added to the Cu/Co/Mn solution drop by drop with constant stirring for 30 min. Moreover, the produced precipitate was separated, washed several times with distilled water, and dried at 60 °C for 24 hrs. Additionally, the dried precipitate was ignited at 550 °C for 4 hrs.

2.3. Instrumentation

Using a PANalytical XRD diffractometer with Kα Cu line equal to 1.5 Å, the average crystallite size and crystal structure of the P_1 and P_2 composites were determined. Using an Ultra 55 Gemini-Zeiss scanning electron microscope, the surface shape and constituents of the P_1 and P_2 composites were determined. Using a Talos F200iS transmission electron microscope, the morphologies of the P_1 and P_2 composites were obtained. The surface textures of the P_1 and P_2 composites were determined using a Quantachrome TouchWin nitrogen gas sorption analyzer after 12 hrs of degassing at 60 °C. The energy gap of the P_1 and P_2 composites and concentration of the malachite green dye was obtained using a Shimadzu-M160 PC UV–vis spectrophotometer. Maximum malachite green dye wavelength is 620 nm.

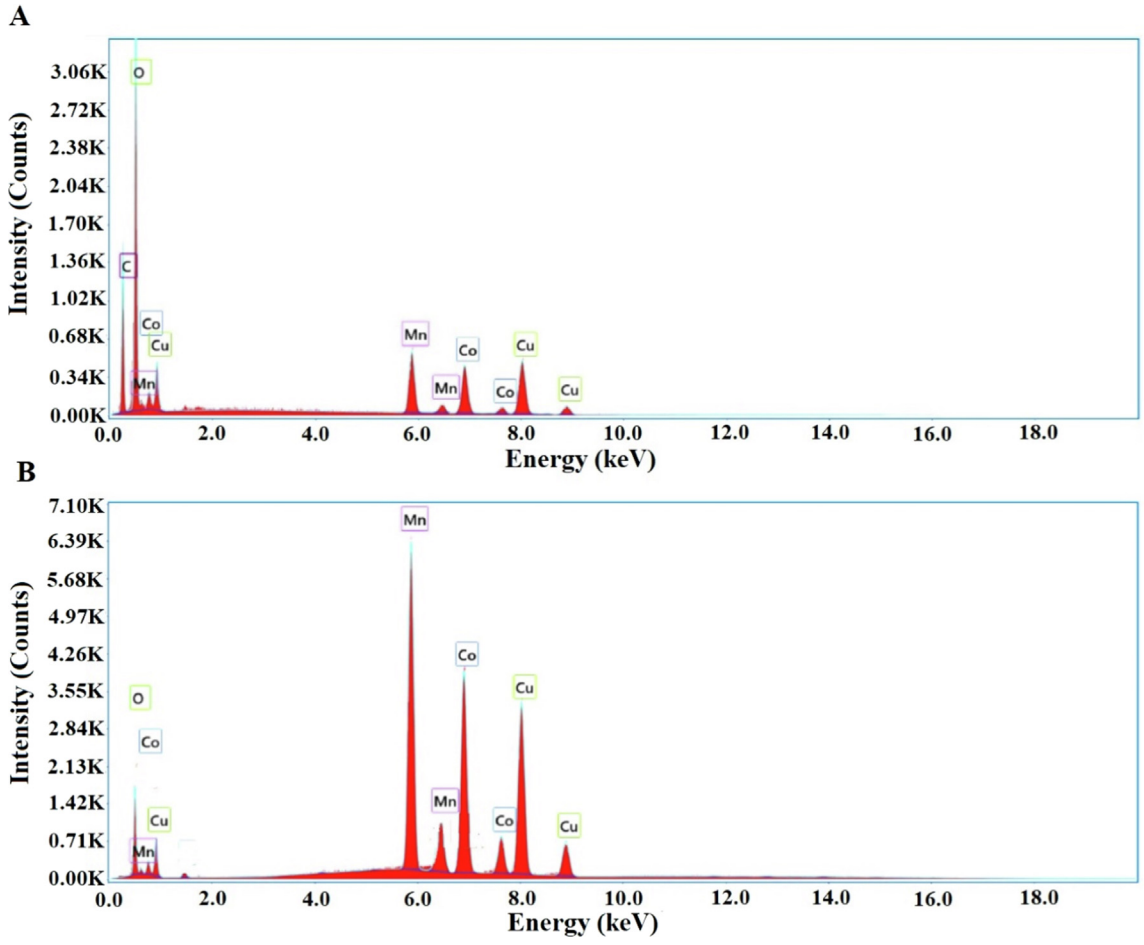

Fig. 2 EDX patterns of the P_1 (A) and P_2 (B) composites.

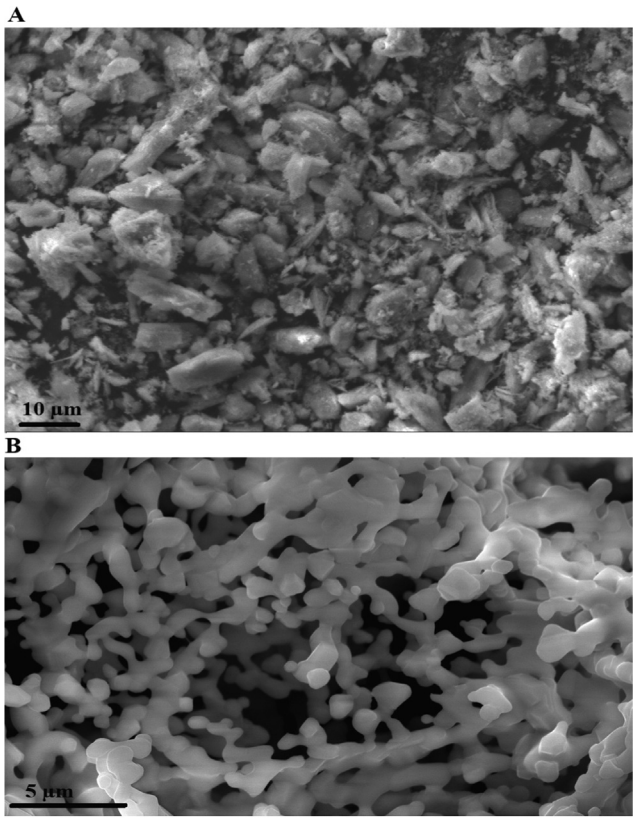

Fig. 3 Scanning electron microscope images of the P_1 (A) and P_2 composites.

2.4. Photocatalytic degradation of malachite green dye

The P_1 or P_2 catalyst is combined with the malachite green dye solution in a 250 mL beaker and stirred for 4 hrs in a dark location. During stirring, the beaker is then exposed to ultraviolet light (Wavelength = 254 nm, Length = 40 cm, Power = 10 Watt). According to Table 1, several parameters impacting the photocatalytic degradation of malachite green dye using the P_1 and P_2 composites have been examined.

The preceding experimental procedures were repeated with the addition of 0.5 mL of a 1 M hydrogen peroxide solution. In the instance of regeneration and reusability, the P_1 or P_2 catalysts were regenerated by washing them with hot distilled water after every cycle and then drying them at 60 °C. Four cycles were then utilized for the degradation of the malachite green dye.

The percentage of photocatalytic degradation (% Degradation Efficiency) of malachite green dye was calculated using Eq. (1).

$$\%\,\text{Degradation Efficiency} = \frac{B_0 - B_e}{B_o} \times 100 \quad (1)$$

B_o (mg/L) is the concentration of the malachite green dye after the end of its stirring period in a dark place. B_e (mg/L) is the concentration of the malachite green dye after the expiration of the period of stirring in the presence of ultraviolet rays.

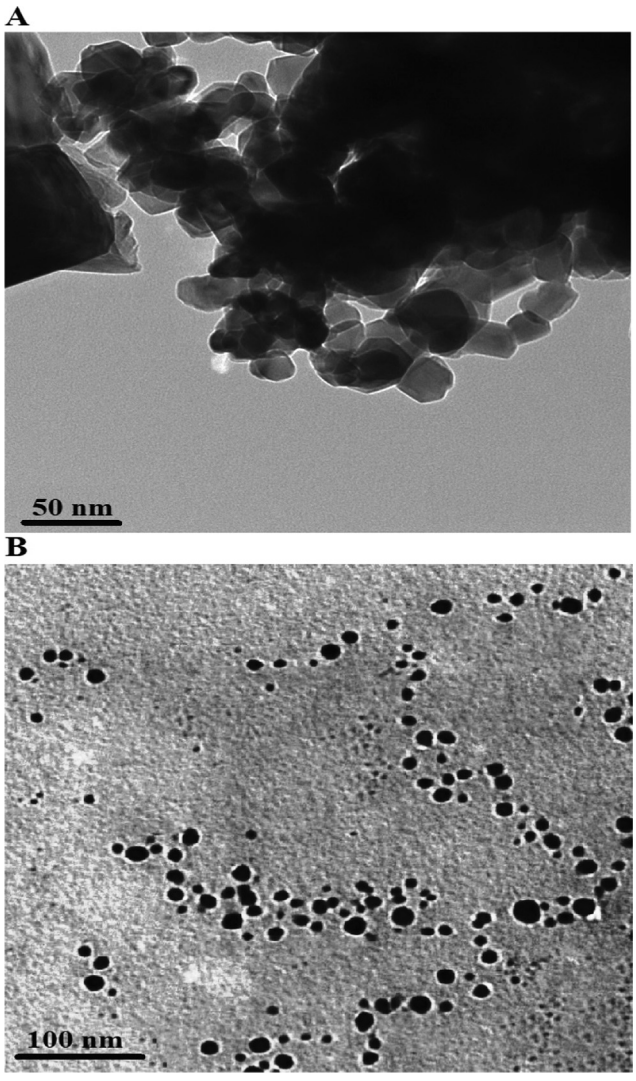

Fig. 4 Transmission electron microscope images of the P_1 (A) and P_2 composites.

3. Results and discussion

3.1. Characterization of the synthesized composites

The appearance of XRD peaks at 2Θ = 18.84°, 22.79°, 24.66°, 30.05°, 33.58°, and 34.62° confirms that the P_1 composite consists of copper oxalate hydrate ($CuC_2O_4{\cdot}H_2O$, JCPDS No. 00–022-1089), cobalt oxalate hydrate ($CoC_2O_4{\cdot}2H_2O$, JCPDS No. 00–025-0250), and manganese oxalate hydrate ($MnC_2O_4{\cdot}2H_2O$, JCPDS No. 00–025-0544) as clarified in Fig. 1A. Also, the P_2 composite consists of copper oxide (CuO, JCPDS No. 00–005-0661), cobalt manganese oxide ($(Co,Mn)(Co,Mn)_2O_4$, JCPDS No. 00–018-0408), and manganese oxide (Mn_5O_8, JCPDS No. 00–018-0801) as clarified in Fig. 1B. Characteristic peaks of copper oxide appear at 2Θ = 35.69°, 38.91°, 45.77°, 48.93°, 61.70°, and 66.17°. Characteristic peaks of manganese oxide appear at 2Θ = 15.98°, 31.14°, 44.32°, and 64.54°. Characteristic peaks of cobalt manganese oxide appear at 2Θ = 36.

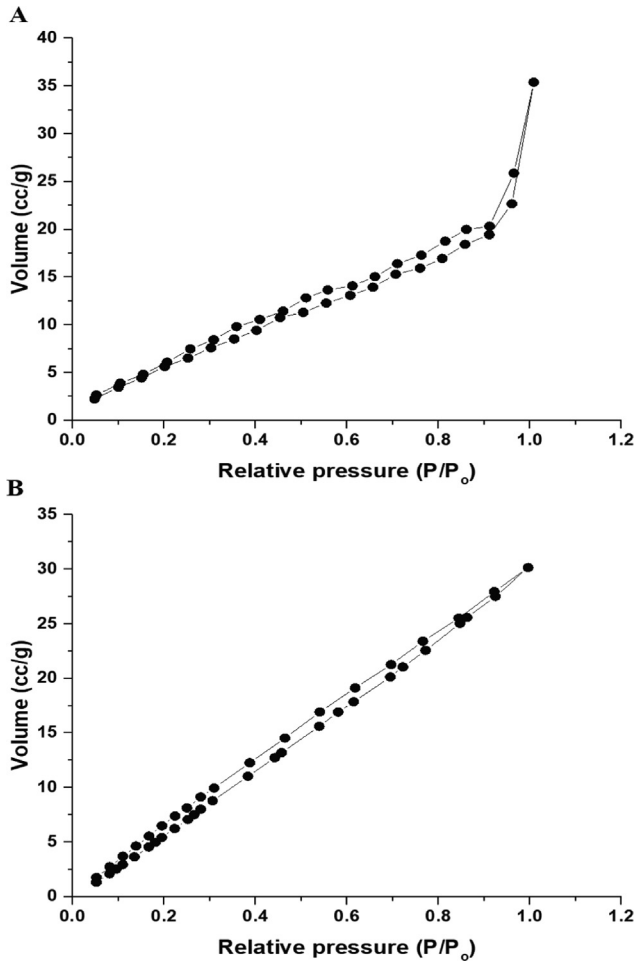

Fig. 5 N_2 adsorption/desorption isotherms of the P_1 (A) and P_2 (B) composites.

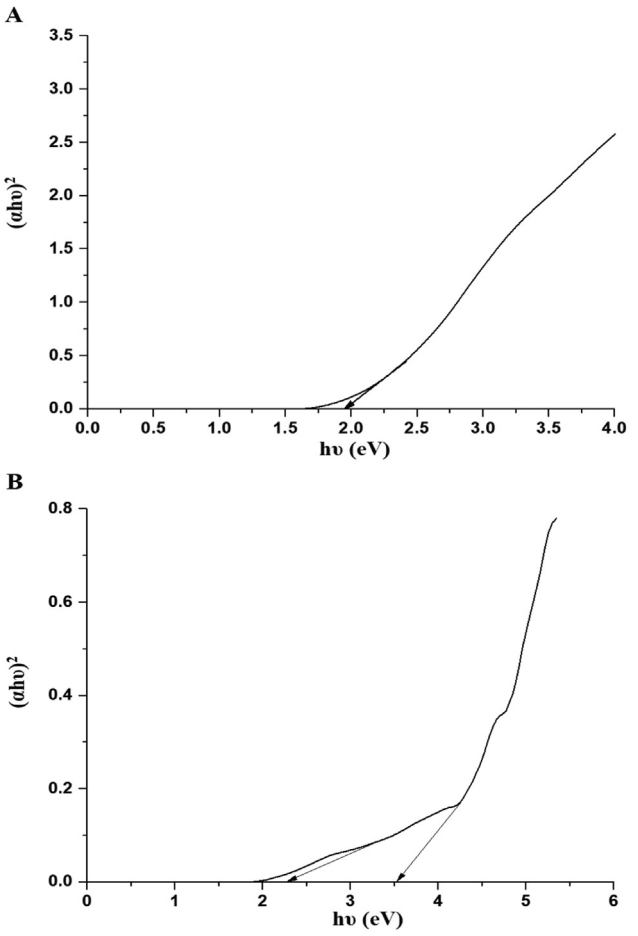

Fig. 6 The plot of $(\alpha h\upsilon)^2$ versus hυ for the P_1 (A) and P_2 (B) composites.

63° and 58.76°. The average crystallite size of the P_1 and P_2 composites is 30.12 and 18.54 nm, respectively.

As seen from EDX spectra in Fig. 2A, the P_1 composite consist of C (26.28 %), oxygen (46.66 %), manganese (7.27 %), cobalt (7.59 %), and copper (12.20 %). Also, the P_2 composite consist of oxygen (8.23 %), manganese (31.34 %), cobalt (27.19 %), and copper (33.24 %) as seen from EDX spectra in Fig. 2B.

A scanning electron microscope shows that the P_1 composite consists of irregular shapes with an average diameter of 3.57 μm, as seen in Fig. 3A. Also, the P_2 composite consists of irregular and spherical shapes with an average diameter of 1.26 μm, as seen in Fig. 3B. A transmission electron microscope shows that the P_1 and P_2 composites consist of polyhedral and spherical shapes with an average diameter of 28.13 and 14.37 nm, as seen in Fig. 4A-B, respectively.

The N_2 adsorption/desorption isotherms of the P_1 and P_2 composites belong to type IV as seen in Fig. 5A-B, respectively (Abdelrahman et al., 2019b). Also, the BET surface area, average pore size, and total pore volume of the P_1 composite are 29.0725 m^2/g, 2.0749 nm, and 0.0302 cc/g, respectively. Besides, the BET surface area, average pore size, and total pore volume of the P_2 composite are 58.1088 m^2/g, 1.6087 nm, 0.0467 cc/g, respectively.

By exploiting the spectrum of the P_1 and P_2 composites in paraffin oil, the optical energy gap (E_{gap}) was calculated using Eq. (2) (Abdelrahman et al., 2019b; Hegazey et al., 2020).

$$(\alpha h\upsilon)P = Ko\,(h\upsilon - Egap) \quad (2)$$

K_o, α, P are a constant, the absorption coefficient, and an integer based on the nature of the transition. P = 0.5 for indirect permitted transitions, whereas P = 2 for direct permitted transitions. As seen in Fig. 6A-B, direct permitted transitions predominated in the P_1 and P_2 composites. The energy gap of the P_1 composite is 1.96 eV. Also, the energy gaps of the P_2 composite are 2.29 and 3.53 eV.

3.2. Photocatalytic degradation of malachite green dye

3.2.1. Effect of pH

The effect of pH on the degradation efficiency of malachite green dye using the P_1 and P_2 composites was studied with pH varying from 2.5 to 8.5 as seen in Fig. 7A-B, respectively. The optimal pH for the degradation of malachite green dye in the absence and presence of hydrogen peroxide is 8.5. The degradation efficiency of malachite green dye, at pH = 8.5 using the P_1 composite in the absence and presence of hydrogen peroxide, is 29.58 and 100 %, respectively. The degrada-

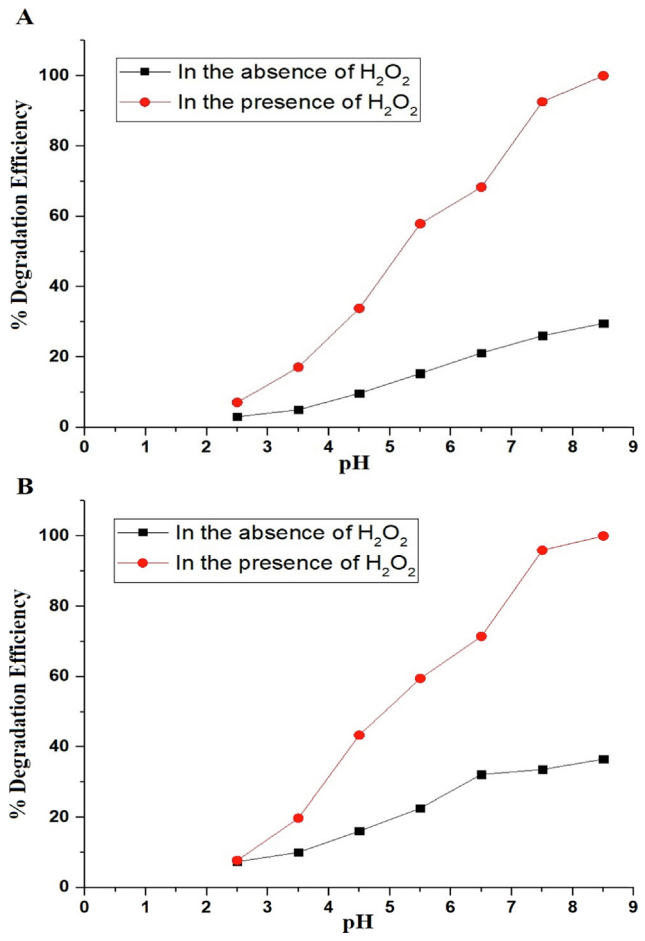

Fig. 7 The effect of pH on the degradation efficiency of malachite green dye using the P_1 (A) and P_2 (B) composites.

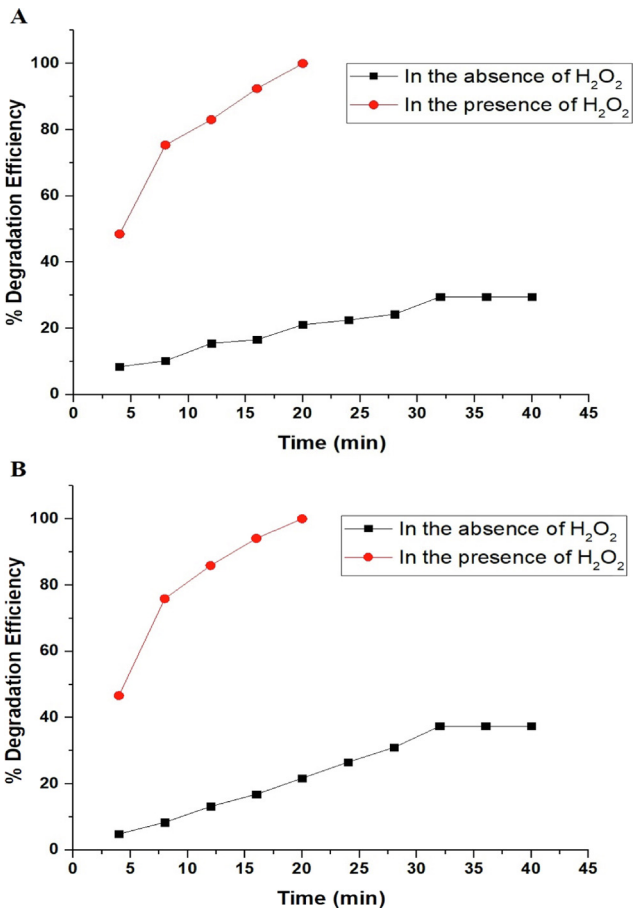

Fig. 8 The effect of time on the degradation efficiency of malachite green dye using the P_1 (A) and P_2 (B) composites.

tion efficiency of malachite green dye, at pH = 8.5 using the P_2 composite in the absence and presence of hydrogen peroxide, is 36.50 and 100 %, respectively. The ability of hydrogen peroxide under the effect of UV rays to form more hydroxyl free radicals, which accelerate the degradation of the malachite green dye, boosted the degradation efficiency as compared to the absence of hydrogen peroxide. The point of zero charge of the P_1 and P_2 composites was determined as described by Khalifa et al (Khalifa et al., 2020). The point of zero charge (pH_{PZC}) of the P_1 and P_2 composites is 3.96 and 4.28, respectively. Malachite green dye is a cationic dye. Due to the attraction forces, it is therefore adsorbable on the surface of a catalyst at pH values greater than pH_{PZC}. Thus, the efficiency of malachite green dye degradation improves at pH values greater than pH_{PZC}. Malachite green dye is a cationic dye. Consequently, electrostatic repulsion prevents it from being favorably adsorbed on the surface of a catalyst at pH values below pH_{PZC}. Thus, at pH levels below pH_{PZC}, the degradation efficiency of malachite green dye decreases (Abdelwahab et al., 2022).

3.2.2. Effect of time

The effect of time on the degradation efficiency of malachite green dye using the P_1 and P_2 composites was studied with time varying from 4 min to 40 min as seen in Fig. 8A-B, respectively. The optimal period for the degradation of malachite green dye utilizing the P_1 and P_2 composites in the absence of hydrogen peroxide was determined to be 32 min. Due to the saturation of the active sites, it was observed that the degradation efficiency of malachite green dye remains rather stable when the irradiation time increases from 32 min to 40 min. The optimal period for the degradation of malachite green dye utilizing the P_1 and P_2 composites in the presence of hydrogen peroxide was determined to be 20 min. In the absence of hydrogen peroxide, the degradation efficiency of malachite green dye using the P_1 and P_2 composites is 29.58 and 37.39 %, respectively. In the presence of hydrogen peroxide, the degradation efficiency of malachite green dye using the P_1 and P_2 composites is 100 %.

Using Eq. (3), the photocatalytic degradation processes of malachite green dye using the P_1 and P_2 composites were found to obey the first-order kinetic model as seen in Fig. 9-A-B, respectively (Abdelwahab et al., 2022).

$$ln(Bo/Be) = K1t \tag{3}$$

where, K_1 (1/min) and t (min) are the constant of first order kinetic model and irradiation time, respectively. The K values and correlation coefficients (R^2) are listed in Table 2.

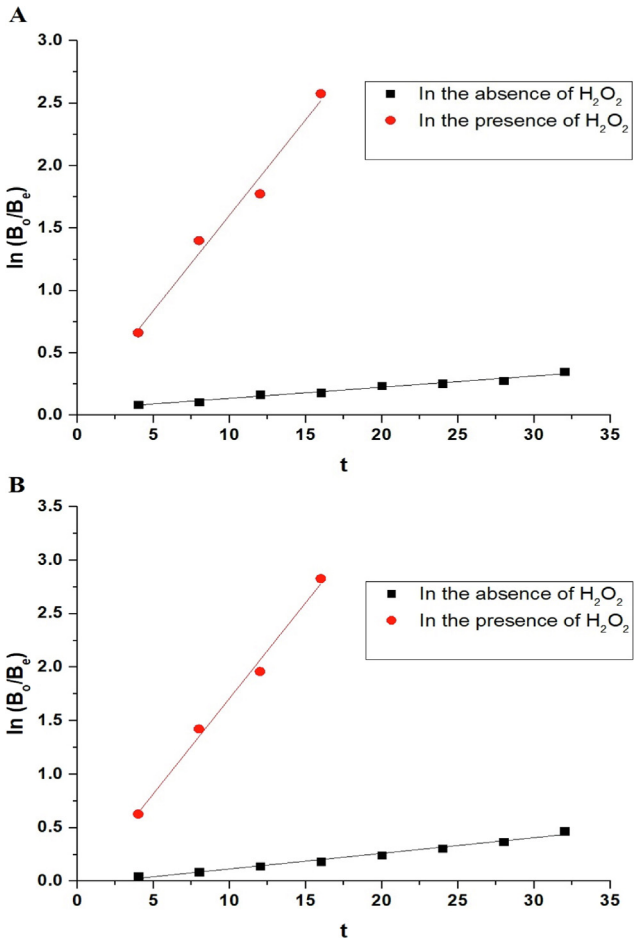

Fig. 9 The plots of ln (B_o/B_e) versus irradiation time using the P_1 (A) and P_2 (B) composites.

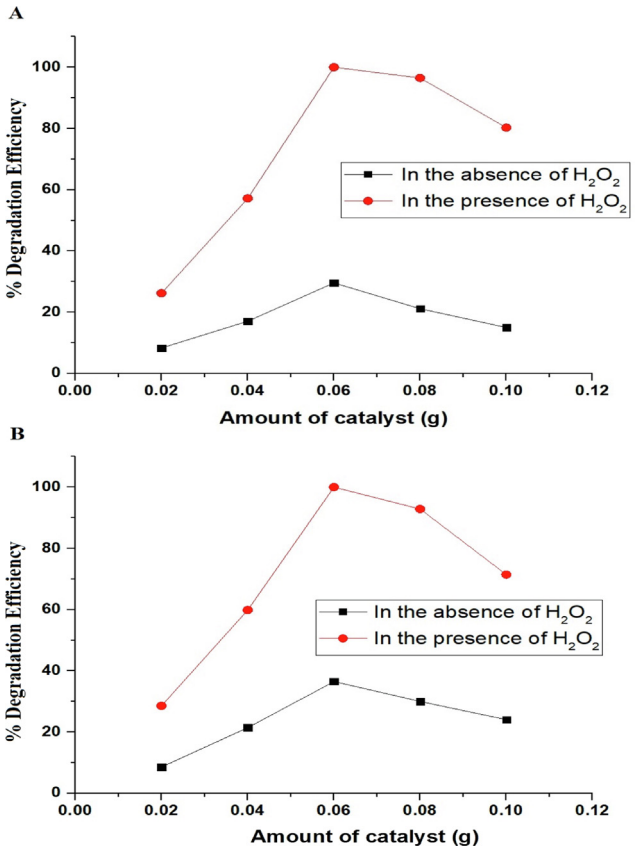

Fig. 10 The effect of amount of catalyst on the degradation efficiency of malachite green dye using the P_1 (A) and P_2 (B) composites.

3.2.3. Effect of amount of catalyst

The effect of amount of catalyst on the degradation efficiency of malachite green dye using the P_1 and P_2 composites was studied with amount varying from 0.02 g to 0.10 g as seen in Fig. 10A-B, respectively. The optimal amount of catalyst for the degradation of malachite green dye utilizing the P_1 and P_2 composites was determined to be 0.06 g due to the increase in the number of catalyst particles, which improves photon absorption. In addition, it was noticed that the degradation efficiency of malachite green dye decreased when the amount of catalyst was increased from 0.06 g to 0.10 g due to the screening of incident light by the excess catalyst particles and the catalyst aggregation (Abdelwahab et al., 2022).

3.2.4. Effect of initial malachite green dye concentration

The effect of initial concentration of malachite green dye on the degradation efficiency using the P_1 and P_2 composites was studied with concentration varying from 5 mg/L to 25 mg/L as seen in Fig. 11A-B, respectively. In addition, it was observed that the degradation efficiency of malachite green dye decreases as the dye concentration increases from 5 mg/L to 25 mg/L. This is as a result of the shorter path length of photons entering the malachite green dye solution, which limits photon absorption by the catalyst and, consequently, photocatalytic degradation (Abdelwahab et al., 2022).

3.2.5. Effect of regeneration and reusability

The effect of regeneration and reusability on the degradation efficiency of malachite green dye using the P_1 and P_2 composites was studied for four cycles as seen in Fig. 12A-B, respectively. The results indicated that the degradation efficiency of malachite green dye has been slightly modified. This shows that these catalysts can be utilized repeatedly without diminishing in efficacy.

Table 2 The constants of the first order reaction of the degradation of malachite green dye using the P_1 and P_2 composites.

Composite	K_1 (1/min)		R^2	
	Without H_2O_2	With H_2O_2	Without H_2O_2	With H_2O_2
P_1	0.0089	0.1529	0.9735	0.9743
P_2	0.01461	0.1784	0.9814	0.9891

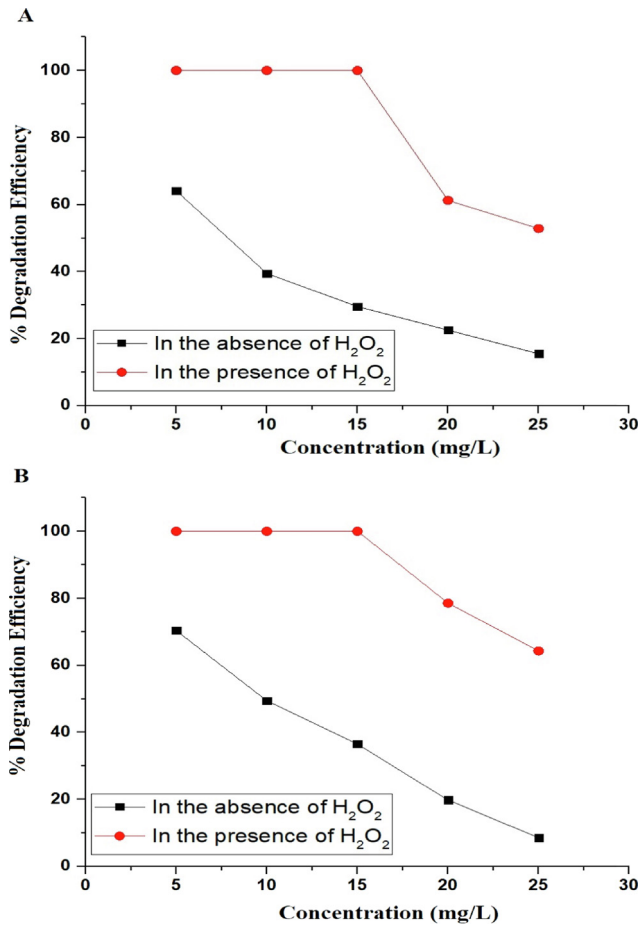

Fig. 11 The effect of malachite green dye concentration on the degradation efficiency using the P_1 (A) and P_2 (B) composites.

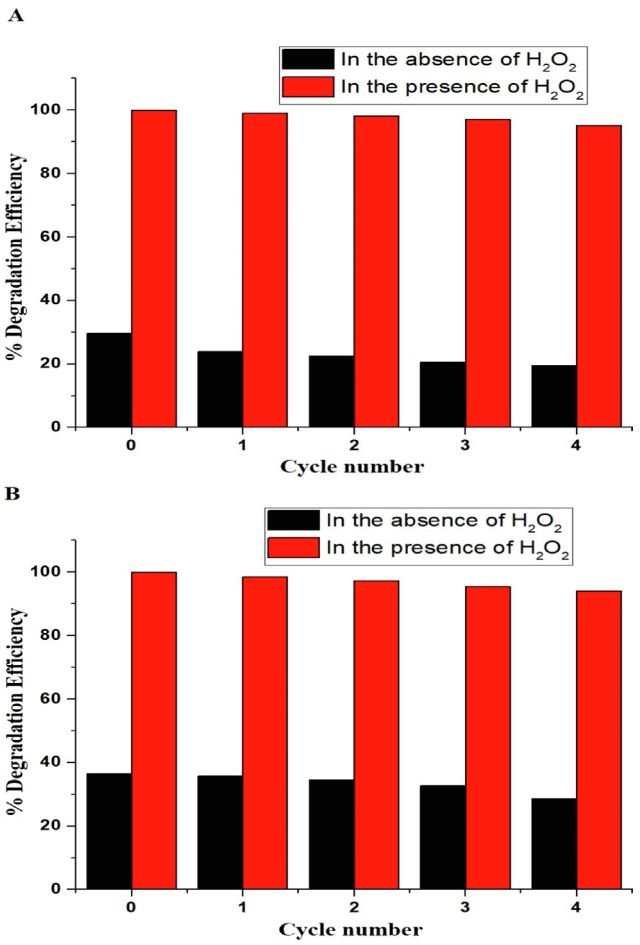

Fig. 12 The effect of regeneration and reusability on the degradation efficiency of malachite green dye using the P_1 (A) and P_2 (B) composites.

3.2.6. Mechanism of photocatalytic degradation of malachite green dye

As illustrated in Fig. 13, when UV rays excite electrons in the valence band, they transfer to the conduction band, resulting in the production of holes at the valence band and electrons at the conduction band. The conduction and valence bands then produced oxygen anion free radicals ($O_2^{\cdot-}$) and hydroxyl free radicals ($^{\cdot}OH$), respectively. Free radicals eventually convert malachite green dye to volatile gases (CO_2 and H_2O). Hydrogen peroxide inhibits the rapid recombination of electrons and holes and increases the quantity of hydroxyl free radicals. Therefore, this addition improves the catalytic efficiency of malachite green dye degradation (Abdelwahab et al., 2022).

3.2.7. Comparison of photocatalytic degradation of malachite green dye using the produced composites with other photocatalysts

As clarified in Table 3, the photocatalytic degradation of malachite green dye using the P_1 and P_2 composites has been compared with that of other photocatalysts reported in the literature such as Fe(III)-cross-linked alginate-carboxymethyl cellulose composite (Karadeniz et al., 2022), cobalt oxide/citric acid nanocomposite (Verma et al., 2021), sn-doped TiO_2 (Sayilkan et al., 2007), Fe_3O_4/ SiO_2/TiO_2 composite (Farhadian and Kazemzad, 2016), and chitosan supported Ce–ZnO (Saad et al., 2020). The results demonstrated that the P_1 and P_2 composites are superior to other catalysts in their capacity to rapidly degrade a significant volume and concentration of malachite green dye.

4. Conclusions

Copper oxalate/cobalt oxalate/manganese oxalate (Abbreviated as P_1) and copper oxide/cobalt manganese oxide/manganese oxide (Abbreviated as P_2) new nanocomposites were fabricated via precipitation of Cu^{2+}/Co^{2+}/Mn^{2+} solution using oxalic acid and ignition of precipitate at 550 °C for 4 hrs, respectively. The average crystallite size of the $P1$ and $P2$ composites is 30.12 and 18.54 nm, respectively. The $P1$ composite consist of C (26.28 %), oxygen (46.66 %), manganese (7.27 %), cobalt (7.59 %), and copper (12.20 %). Also, the $P2$ composite consist of oxygen (8.23 %), manganese (31.34 %), cobalt (27.19 %), and copper (33.24 %). The $P1$ composite consists of irregular shapes with an average diameter of 3.57 μm. The $P2$ composite consists of irregular and spherical shapes with an average diameter of 1.26 μm. 60 mg of the synthesized nanocomposites completely decompose 60 mL of 15 mg/L of malachite green dye solution within 20 min in the presence of hydrogen peroxide and UV light.

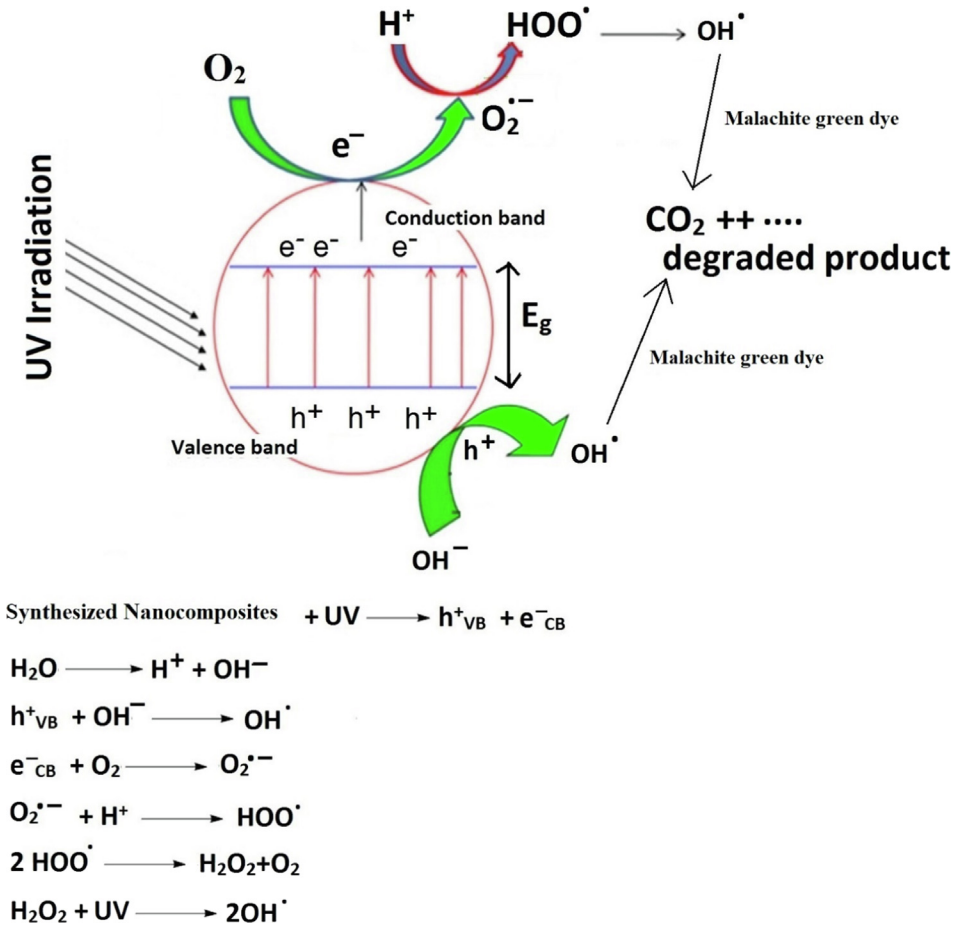

Fig. 13 The suggested mechanism for the degradation of malachite green dye.

Table 3 Comparison between the photocatalytic degradation of malachite green dye and that of other photocatalysts.

Catalyst	Amount of catalyst (g)	Concentration of dye (mg/L)	Volume of dye (mL)	% Degradation	Time (min)	Ref
Fe(III)-cross-linked alginate-carboxymethyl cellulose	0.10	10	50	98.8	30	(Karadeniz et al., 2022)
Cobalt oxide/citric acid	0.05	10	100	91.20	100	(Verma et al., 2021)
Sn-doped TiO_2	0.10	20	25	100	340	(Sayilkan et al., 2007)
Fe_3O_4/ SiO_2/TiO_2	0.10	10	100	100	150	(Farhadian and Kazemzad, 2016)
Chitosan supported Ce–ZnO	0.02	5	100	83	180	(Saad et al., 2020)
P_1	0.06	15	60	100	20	This work
P_2	0.06	15	60	100	20	This work

Declaration of Competing Interest

The authors declare that they have no known competing financial interests or personal relationships that could have appeared to influence the work reported in this paper.

References

Abdelrahman, E.A., 2018. Synthesis of zeolite nanostructures from waste aluminum cans for efficient removal of malachite green dye from aqueous media. J. Mol. Liq. 253, 72–82. https://doi.org/10.1016/j.molliq.2018.01.038.

Abdelrahman, E.A., Hegazey, R.M., 2019. Facile synthesis of HgO nanoparticles using hydrothermal method for efficient photocatalytic degradation of crystal violet dye under UV and sunlight irradiation. J. Inorg. Organomet. Polym. Mater. 29. https://doi.org/10.1007/s10904-018-1005-6.

Abdelrahman, E.A., Hegazey, R.M., El-Azabawy, R.E., 2019a. Efficient removal of methylene blue dye from aqueous media using Fe/Si, Cr/Si, Ni/Si, and Zn/Si amorphous novel adsorbents. J. Mater. Res. Technol. 8, 5301–5313. https://doi.org/10.1016/j.jmrt.2019.08.051.

Abdelrahman, E.A., Hegazey, R.M., Kotp, Y.H., Alharbi, A., 2019b. Facile synthesis of Fe2O3 nanoparticles from Egyptian insecticide cans for efficient photocatalytic degradation of methylene blue and

crystal violet dyes. Spectrochim. Acta - Part A Mol. Biomol. Spectrosc. 222,. https://doi.org/10.1016/j.saa.2019.117195 117195.

Abdelwahab, M.A., Rayes, S.M.E., Kamel, M.M., Ehab, A., 2022. Encapsulation of NiS and ZnS in analcime nanoparticles as novel nanocomposites for the effective photocatalytic degradation of orange G and methylene blue dyes Encapsulation of NiS and ZnS in analcime nanoparticles as novel nanocomposites for the effectiv. Int. J. Environ. Anal. Chem. 00, 1–18. https://doi.org/10.1080/03067319.2022.2100260.

Adel, M., Ahmed, M.A., Elabiad, M.A., Mohamed, A.A., 2022. Removal of heavy metals and dyes from wastewater using graphene oxide-based nanomaterials: a critical review. Environ. Nanotechnology, Monit. Manag. 18,. https://doi.org/10.1016/j.enmm.2022.100719 100719.

Alharbi, A., Abdelrahman, E.A., 2020. Efficient photocatalytic degradation of malachite green dye using facilely synthesized hematite nanoparticles from Egyptian insecticide cans. Spectrochim. Acta - Part A Mol. Biomol. Spectrosc. 226,. https://doi.org/10.1016/j.saa.2019.117612 117612.

AL-Harbi, L.M., Darwish, M.S.A., 2022. Functionalized iron oxide nanoparticles: synthesis through ultrasonic-assisted co-precipitation and performance as hyperthermic agents for biomedical applications. Heliyon 8, e09654. https://doi.org/10.1016/j.heliyon.2022.e09654.

Altiner, M., Top, S., Bouchekrit, C., Kursunoglu, S., 2022. Production of Mn3O4 nanoparticles from a manganiferous iron ore via reductive leaching, precipitation, and calcination. Hydrometallurgy 208, 105810. https://doi.org/10.1016/j.hydromet.2021.105810.

Aseena, S., Abraham, N., Suresh Babu, V., 2021. Morphological and optical studies of zinc doped cerium oxide nanoparticles prepared by single step co-precipitation method. Mater. Today Proc. https://doi.org/10.1016/j.matpr.2021.05.636.

Bi, R., Yin, D., Lei, B., Chen, F., Zhang, R., Li, W., 2022. Mercaptocarboxylic acid intercalated MgAl layered double hydroxide adsorbents for removal of heavy metal ions and recycling of spent adsorbents for photocatalytic degradation of organic dyes. Sep. Purif. Technol. 289,. https://doi.org/10.1016/j.seppur.2022.120741 120741.

Farhadian, M., Kazemzad, M., 2016. Photocatalytic degradation of malachite green by magnetic photocatalyst. Synth. React. Inorg. Met. Nano-Metal Chem. 46, 458–463. https://doi.org/10.1080/15533174.2014.988802.

Hegazey, R.M., Abdelrahman, E.A., Kotp, Y.H., Hameed, A.M., Subaihi, A., 2020. Facile fabrication of hematite nanoparticles from Egyptian insecticide cans for efficient photocatalytic degradation of rhodamine B dye. J. Mater. Res. Technol. 9, 1652–1661. https://doi.org/10.1016/j.jmrt.2019.11.090.

Karadeniz, D., Kahya, N., Erim, F.B., 2022. Effective photocatalytic degradation of malachite green dye by Fe(III)-Cross-linked Alginate-Carboxymethyl cellulose composites. J. Photochem. Photobiol. A Chem. 428, 113867. https://doi.org/10.1016/j.jphotochem.2022.113867.

Khalifa, M.E., Abdelrahman, E.A., Hassanien, M.M., Ibrahim, W.A., 2020. Application of mesoporous silica nanoparticles modified with Dibenzoylmethane as a novel composite for efficient removal of Cd (II), Hg(II), and Cu(II) ions from aqueous media. J. Inorg. Organomet. Polym. Mater. 30, 2182–2196. https://doi.org/10.1007/s10904-019-01384-w.

Kumar, A., Gangawane, K.M., 2022. Effect of precipitating agents on the magnetic and structural properties of the synthesized ferrimagnetic nanoparticles by co-precipitation method. Powder Technol. 401,. https://doi.org/10.1016/j.powtec.2022.117298 117298.

Mahmood, N.B., Saeed, F.R., Gbashi, K.R., Mahmood, U.S., 2022. Synthesis and characterization of zinc oxide nanoparticles via oxalate co-precipitation method. Mater. Lett. X 13,. https://doi.org/10.1016/j.mlblux.2022.100126 100126.

Raval, N.P., Shah, P.U., Shah, N.K., 2017. Malachite green "a cationic dye" and its removal from aqueous solution by adsorption. Appl. Water Sci. 7, 3407–3445. https://doi.org/10.1007/s13201-016-0512-2.

Rayaroth, M.P., Oh, D., Lee, C.S., Chang, Y.S., 2022. Simultaneous removal of heavy metals and dyes in water using a MgO-coated Fe3O4 nanocomposite: role of micro-mixing effect induced by bubble generation. Chemosphere 294,. https://doi.org/10.1016/j.chemosphere.2022.133788 133788.

Saad, A.M., Abukhadra, M.R., Abdel-Kader Ahmed, S., Elzanaty, A. M., Mady, A.H., Betiha, M.A., Shim, J.J., Rabie, A.M., 2020. Photocatalytic degradation of malachite green dye using chitosan supported ZnO and Ce–ZnO nano-flowers under visible light. J. Environ. Manage. 258,. https://doi.org/10.1016/j.jenvman.2019.110043 110043.

Sayilkan, F., Asiltürk, M., Tatar, P., Kiraz, N., Arpaç, E., Sayilkan, H., 2007. Photocatalytic performance of Sn-doped TiO2 nanostructured mono and double layer thin films for Malachite Green dye degradation under UV and vis-lights. J. Hazard. Mater. 144, 140–146. https://doi.org/10.1016/j.jhazmat.2006.10.011.

Sujatha, K., Sharmila, S., Sudha, A.P., Shanmugasundaram, O.L., 2021. Surfactant assisted spectroscopic application of cadmium oxide nanoparticles prepared via co-precipitation method. Mater. Today Proc. 50, 48–52. https://doi.org/10.1016/j.matpr.2021.03.626.

Sun, M., Fang, Q., Li, Z., Cai, C., Li, H., Cao, B., Shen, W., Liu, T.X., Fu, Y.Q., 2021. Co-precipitation synthesis of CuCo2O4 nanoparticles for supercapacitor electrodes with large specific capacity and high rate capability. Electrochim. Acta 397,. https://doi.org/10.1016/j.electacta.2021.139306 139306.

Verma, M., Mitan, M., Kim, H., Vaya, D., 2021. Efficient photocatalytic degradation of Malachite green dye using facilely synthesized cobalt oxide nanomaterials using citric acid and oleic acid. J. Phys. Chem. Solids 155,. https://doi.org/10.1016/j.jpcs.2021.110125 110125.

Wang, T., Aguey-Zinsou, K.F., 2021. Synthesis of borohydride nanoparticles at room temperature by precipitation. Int. J. Hydrogen Energy 46, 24286–24292. https://doi.org/10.1016/j.ijhydene.2021.05.001.